

Acute Lymphoblastic Leukemia Classification from Microscopic Images using Convolutional Neural Networks

Jonas Prellberg and Oliver Kramer

University of Oldenburg, Oldenburg, Germany
`{jonas.prellberg,oliver.kramer}@uni-oldenburg.de`

Abstract. Examining blood microscopic images for leukemia is necessary when expensive equipment for flow cytometry is unavailable. Automated systems can ease the burden on medical experts for performing this examination and may be especially helpful to quickly screen a large number of patients. We present a simple, yet effective classification approach using a ResNeXt convolutional neural network with Squeeze-and-Excitation modules. The approach was evaluated in the C-NMC online challenge and achieves a weighted F1-score of 88.91 % on the test set. Code is available at <https://github.com/jprellberg/isbi2019cancer>.

1 Introduction

Acute lymphoblastic leukemia (ALL) is a blood cancer that is characterized by the proliferation of abnormal lymphoblast cells, eventually leading to the accumulation of a lethal number of leukemia cells [12]. If ALL is diagnosed in an early stage, treatment is possible. Diagnosis is typically performed using a complete blood count and morphological analysis of cells under a microscope by a medical expert. Flow cytometry can replace this manual work but requires expensive equipment which is not available everywhere. Therefore, automated systems that can perform diagnosis using comparatively low-cost microscopic images provide a great advantage.

To further research in this direction, public datasets are necessary to compare different approaches and track the state-of-the-art. A popular example for single-cell ALL classification is ALL-IDB2 [9], but with only 260 images of white blood cells the dataset is too small to properly take advantage of recent deep learning approaches. In 2018, a new dataset with more than 10,000 training images and a separate test set of normal B-lymphoid precursors and malignant B-lymphoblasts has been released as an online challenge¹ open to the public. The large size of this new dataset allows to create improved classifiers based on deep neural networks and also provides a more reliable comparison of competing approaches.

In this work we present our approach to the classification of healthy and malignant cells on the mentioned dataset using a convolutional neural network.

¹ <https://competitions.codalab.org/competitions/20429>

In Section 2 the dataset is described in more detail and our data augmentation strategy is outlined. The convolutional neural network, a ResNeXt-variant with Squeeze-and-Excitation modules, is presented in Section 3. In Section 4 we describe the training process and show experimental results. A summary of related work and a conclusion follow.

2 Dataset

The challenge dataset [5,6,4,2,3], hereafter referred to as C-NMC dataset, contains images of white blood cells taken from 154 individual subjects, 84 of which exhibit ALL. Table 1 provides a detailed breakdown of the number of subjects and cells in training and test sets. The dataset is imbalanced with about twice as many ALL cells as normal cells.

Each image has a resolution of 450×450 pixels and contains only a single cell as a consequence of preprocessing steps applied by the dataset authors: An automated segmentation algorithm has been used to separate the cells from the background. Each pixel that was determined not to be part of the cell is colored completely black. However, since the segmentation algorithm is not perfect, there are instances where parts of the cell are inadvertently colored black or superfluous background is included. Additionally, all images have been preprocessed with a stain-normalization procedure that performs white-balancing and fixes errors introduced due to variations in the staining chemical [6]. See Figure 1 for example images from the dataset.

Table 1: Composition of the dataset. At the time of writing the ground truth for the final test set is not yet released, so some information is missing.

Dataset part	ALL subjects	Normal subjects	ALL cells	Normal cells
Train	47	26	7272	3389
Prelim. test	13	15	1219	648
Final test	9	8	?	?

Even though the dataset contains more than 10,000 images, several data augmentation techniques can be applied to increase the amount of training data further and improve the training of our convolutional neural network. Since microscopic images are invariant to flips and rotations, we perform horizontal and vertical flips with 50 % probability each and rotations with an angle from $[0, 360)$ degrees chosen uniformly at random. Since convolutional neural networks with pooling operations or strides larger than one are not perfectly translation

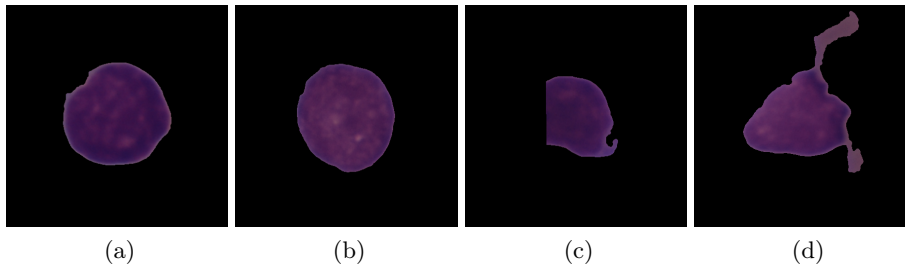


Fig. 1: Example images taken from the training set. **(a)** ALL cell **(b)** Normal cell **(c)** ALL cell with part of the cell cut off due to an imperfect segmentation **(d)** Normal cell with superfluous background due to an imperfect segmentation

invariant, we also perform random translations of up to 20 % of each side-length in horizontal and vertical directions.

We do not randomly scale the images because cell size may be a diagnostic factor to differentiate between ALL and normal cells [1]. Furthermore, we do not apply any brightness or color augmentation due to this dataset’s stain-normalization preprocessing. Both data augmentation methods are commonly used but would lead to an unnecessary distribution shift between training and test set on this specific dataset.

Additionally, the images are center-cropped to 300×300 pixels to decrease the dimensionality of the input data. This will generally make learning a classifier faster and easier. Even though the cropping discards large parts of the image, it has no effect on the classification accuracy because only very few cells are actually larger than this crop. In many cases, images that are not completely black outside of the crop are segmentation failures that include parts of the background.

3 Network Architecture

Image classification benchmarks have driven the creation of many powerful convolutional neural network architectures. We pick one of the recent top-performing networks, a ResNeXt50 [18], as our base model. The network consists of five convolutional stages with spatial downsampling by a factor of 2 in between stages, followed by global average pooling and a linear classifier. Each stage is made from stacked building blocks, each of which computes a function of the form

$$x' = x + \sum_{i=1}^C \mathcal{T}_i(x)$$

where C is called the cardinality that controls the number of parallel paths in a block and $\mathcal{T}_i(x)$ is a function that projects x into a lower-dimensional space, transforms it and projects back into a space of the original dimensionality. The

functions $\mathcal{T}_i(x)$ are implemented using a sequence of 1×1 , 3×3 and 1×1 convolutional layers. The block function is modified to

$$x' = x + \text{SE} \left(\sum_{i=1}^C \mathcal{T}_i(x) \right)$$

where SE is the Squeeze-and-Excitation operation introduced in [7], which has been shown to improve performance on image classification benchmarks. In general, the SE operation learns a channel-wise rescaling of feature maps. First, global-average-pooling is applied to the input feature map in order to spatially aggregate the information of each channel. The resulting vector is fed into a two-layer fully-connected network that outputs scale factors. These factors are then used to scale each channel of the original input feature map. More details on the SE-ResNeXt50 architecture can be found in [7].

4 Experiments

The previously described network architecture is used to classify the C-NMC dataset. Since the dataset is imbalanced the overall accuracy can be misleading and we report accuracy, sensitivity and specificity as well as weighted F1-scores, weighted precision and weighted recall. For sensitivity and specificity the ALL-class is regarded as the positive class. Furthermore, because the data is from multiple subjects, we report subject-level accuracies.

Hyperparameters for the training procedure have been chosen by validating on the preliminary test set. The chosen hyperparameters are used for multiple training runs with different random seeds and the best model according to the F1-score on the preliminary test set is selected for our competition entry. Final results on the test set are taken from the online challenge leaderboard.

4.1 Training and Testing

The network is pre-trained on ImageNet [15] and then fine-tuned on the C-NMC training set. The loss function is the weighted binary cross-entropy

$$l(y, \hat{y}) = wy \ln(\sigma(\hat{y})) + (1 - y) \ln(1 - \sigma(\hat{y}))$$

where σ is the sigmoid function, y is the true label, \hat{y} is the network output and $w = n_n/n_p$ is the ratio of negative to positive examples in the training set. The weight w helps to deal with the class imbalance present in the dataset.

The network is fine-tuned for 6 epochs using Adam [8] with a batch size of 16. The learning rate is decayed using a step function that starts at $\eta_{\text{base}} = 1$ and is divided by 10 every 2 epochs. This learning rate is multiplied with factors specific to the part of the network that it is applied to: The first and second stages² have an effective learning rate of $\eta_{12} = 10^{-6}\eta_{\text{base}}$, the third to fifth stages use $\eta_{345} = 10^{-4}\eta_{\text{base}}$ and the last fully connected layer uses $\eta_{\text{fc}} = 10^{-2}\eta_{\text{base}}$.

² Stage refers to a stack of building blocks that operate on the same spatial resolution as described in Section 3 and [18].

This results in lower effective learning rates in the earlier layers of the network and is desirable because the network is initialized with weights from ImageNet pre-training. These have been shown to contain generally useful image filters in the lowest layers [19] and continuing to optimize these weights on a small dataset with large learning rates will degrade these general filters.

During inference, we present 8 rotated versions of each image and average the network output to further improve classification results.

4.2 Model Selection

We find that results are sensitive to the random seed, despite all networks starting from the same weight initialization due to the pre-training. Therefore, we conduct 24 training runs with different random seeds and measure the F1-score on the preliminary test set over the course of the training. We collect the 24 model checkpoints that have the highest F1-scores in their respective training run and report results in Table 2.

The best model achieves an F1-score of 89.81 % on the preliminary test set. Figure 2 shows the evolution of loss and F1-score during its training process, while Figure 3 shows cell classification accuracy grouped by subject. Overall, classification for healthy subjects is worse because the specificity is comparatively low. Consequently, false-positives can be expected when using the network for diagnosis of patients. Still, false-positives are preferable to false-negatives when trying to diagnose cancer with an automated method.

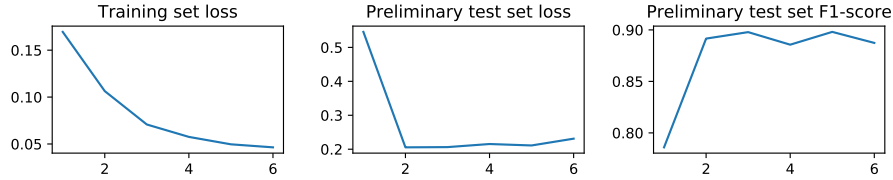


Fig. 2: Training and validation curves of the best model after each training epoch. The model achieves the maximum F1-score after the 5th training epoch.

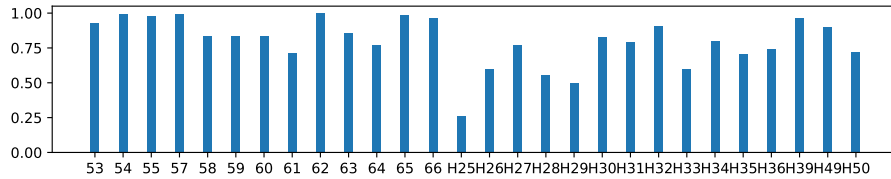


Fig. 3: Subject-level cell classification accuracy on preliminary test set using the best model. Subjects with the prefix H are healthy.

Table 2: Results on the preliminary test set over 24 training runs using the best model of each run measured by F1-score

	Min.	Mean \pm Std.	Max.		Min.	Mean \pm Std.	Max.
Accuracy	86.40	87.96 ± 0.90	89.88	F1-score	86.28	87.89 ± 0.90	89.81
Sensitivity	88.43	92.01 ± 1.44	94.50	Precision	86.27	87.91 ± 0.90	89.81
Specificity	75.31	80.36 ± 2.39	84.72	Recall	86.40	87.96 ± 0.90	89.88

4.3 Results on the Final Test Set

We use the selected model to classify the final test set and submit the result to the online evaluation service. The model achieves a weighted F1-score of 88.91 %.

4.4 Ablation Studies

The main design choices we made for the training and testing procedures are layer-specific learning rates and test-time rotations. In order to show their impact we perform two ablation studies:

NOROT The training procedure is unchanged but during testing the images are only presented in their original orientation.

NOSPECLR During training, every layer has an effective learning rate of $\eta_{\text{all}}\eta_{\text{base}}$ while still using the scheduled decay for η_{base} as described previously. We test $\eta_{\text{all}} \in \{10^{-3}, 10^{-4}, 10^{-5}\}$ and report results for the best setting $\eta_{\text{all}} = 10^{-4}$. The testing procedure is unchanged.

Figure 4 shows results on the preliminary test set for our proposed setting (PROPOSAL) and the two ablation studies. As expected, both ablations decrease performance in terms of all considered metrics. Not using test-time rotations significantly ($p < 0.001$, one-sided Mann-Whitney U test) decreases the mean F1-score from 87.89 ± 0.90 % to 86.92 ± 0.81 %. The influence of layer-wise learning rates is significant ($p < 0.002$) but smaller: A constant learning rate for all layers decreases the mean F1-score to 87.20 ± 0.70 %.

5 Related Work

Previous work on automated ALL diagnosis from images can roughly be divided into more recent approaches that use convolutional neural networks as feature extractors and older approaches that use handcrafted features.

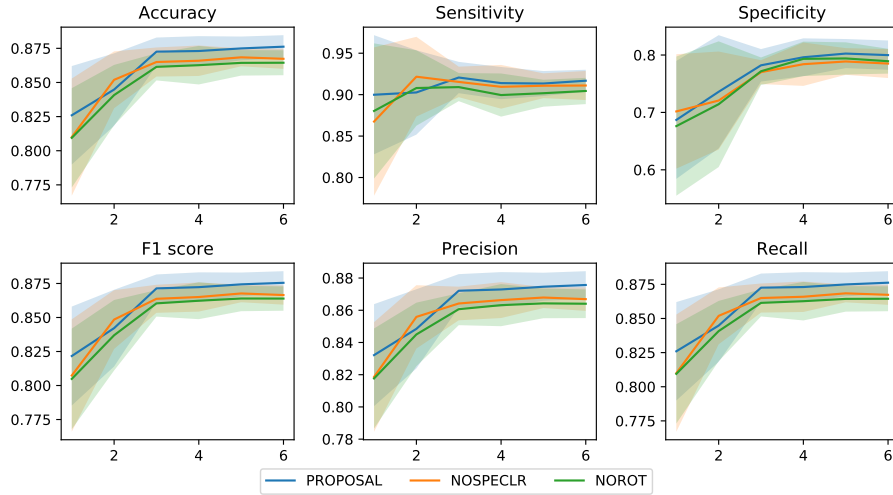


Fig. 4: Metrics on the preliminary test set measured after each training epoch for the proposed setting and the two ablation studies. Lines display the mean over 24 training runs and the shaded area marks one standard deviation. Best viewed electronically and zoomed in.

CNN features. Rehman et al. [14] classify ALL subtypes on a private dataset of 330 images using a pre-trained AlexNet and fine-tuning. Shafique and Tehsin [16] classify ALL subtypes on ALL-IDB augmented with 50 private images, also using a pre-trained AlexNet and fine-tuning. Vogado et al. [17] classify ALL on ALL-IDB using a number of different pre-trained CNNs as fixed feature extractors. From these CNN features the most informative ones are selected using PCA and finally classification is performed with an ensemble of SVM, MLP, and random forest.

Handcrafted features. Putzu and Ruberto [13] use ALL-IDB and classify a number of hand-crafted features like area, compactness, roundness or area ratio between cytoplasm and nucleus with an SVM. Mohapatra et al. [11] and Madhlloom et al. [10] both use (different) private datasets and classify using an ensemble of naive Bayes, KNN, MLP, SVM and a KNN classifier respectively.

All works report good results but it is hardly possible to compare them because the private datasets are unavailable and even on the public ALL-IDB dataset researchers employ their own evaluation procedures. Furthermore, in all cases the employed datasets are small, containing a couple hundred images at most. It is important to have a large dataset that can be used to track the state-of-the-art and we hope that this role can be filled by the C-NMC dataset.

6 Conclusion

We present a simple, yet effective method to automatically classify white blood cell microscopic images into normal B-lymphoid precursors and malignant B-lymphoblasts. A recent convolutional neural network architecture which is fine-tuned on the C-NMC dataset achieves promising classification performance. We hope that the dataset authors release a version with raw images that have not been preprocessed by their in-house methods to allow further research that is not specific to this preprocessing pipeline.

References

1. Chiaretti, S., Zini, G., Bassan, R.: Diagnosis and subclassification of acute lymphoblastic leukemia. *Mediterranean journal of hematology and infectious diseases* **6**(1), e2014073–e2014073 (Nov 2014), <https://www.ncbi.nlm.nih.gov/pubmed/25408859>
2. Duggal, R., Gupta, A., Gupta, R.: Segmentation of overlapping/touching white blood cell nuclei using artificial neural networks. In: *CME Series on Hemato-Oncopathology*. All India Institute of Medical Sciences (AIIMS), New Delhi, India (2016)
3. Duggal, R., Gupta, A., Gupta, R., Mallick, P.: Sd-layer: Stain deconvolutional layer for cnns in medical microscopic imaging. In: Descoteaux, M., Maier-Hein, L., Franz, A., Jannin, P., Collins, D.L., Duchesne, S. (eds.) *Medical Image Computing and Computer Assisted Intervention (MICCAI 2017)*. pp. 435–443. Springer International Publishing, Cham (2017)
4. Duggal, R., Gupta, A., Gupta, R., Wadhwa, M., Ahuja, C.: Overlapping cell nuclei segmentation in microscopic images using deep belief networks. In: *Proceedings of the Tenth Indian Conference on Computer Vision, Graphics and Image Processing*. pp. 82:1–82:8. ICVGIP '16, ACM, New York, NY, USA (2016). <https://doi.org/10.1145/3009977.3010043>, <http://doi.acm.org/10.1145/3009977.3010043>
5. Gupta, A., Duggal, R., Gupta, R., Kumar, L., Thakkar, N., Satpathy, D.: GCTI-SN: Geometry-inspired chemical and tissue invariant stain normalization of microscopic medical images. Under review
6. Gupta, R., Mallick, P., Duggal, R., Gupta, A., Sharma, O.: Stain color normalization and segmentation of plasma cells in microscopic images as a prelude to development of computer assisted automated disease diagnostic tool in multiple myeloma. *Clinical Lymphoma, Myeloma and Leukemia* **17**(1), e99 (2019/03/18 2017)
7. Hu, J., Shen, L., Sun, G.: Squeeze-and-excitation networks. In: *The IEEE Conference on Computer Vision and Pattern Recognition (CVPR)* (June 2018)
8. Kingma, D.P., Ba, J.: Adam: A Method for Stochastic Optimization. *The International Conference on Learning Representations (ICLR '15)* (Dec 2015)
9. Labati, R.D., Piuri, V., Scotti, F.: All-idb: The acute lymphoblastic leukemia image database for image processing. In: *2011 18th IEEE International Conference on Image Processing*. pp. 2045–2048 (Sep 2011). <https://doi.org/10.1109/ICIP.2011.6115881>

10. Madhloom, H.T., Kareem, S.A., Ariffin, H.: A robust feature extraction and selection method for the recognition of lymphocytes versus acute lymphoblastic leukemia. In: 2012 International Conference on Advanced Computer Science Applications and Technologies (ACSAT). pp. 330–335 (Nov 2012). <https://doi.org/10.1109/ACSAT.2012.62>
11. Mohapatra, S., Patra, D., Satpathy, S.: An ensemble classifier system for early diagnosis of acute lymphoblastic leukemia in blood microscopic images. *Neural Computing and Applications* **24**(7), 1887–1904 (Jun 2014). <https://doi.org/10.1007/s00521-013-1438-3>
12. Pui, C.H.: *Acute Lymphoblastic Leukemia*, pp. 39–43. Springer Berlin Heidelberg, Berlin, Heidelberg (2017). https://doi.org/10.1007/978-3-662-46875-3_57
13. Putzu, L., Ruberto, C.D.: White blood cells identification and classification from leukemic blood image. In: International Work-Conference on Bioinformatics and Biomedical Engineering, IWBBIO 2013, Granada, Spain, March 18–20, 2013. Proceedings. pp. 99–106 (2013)
14. Rehman, A., Abbas, N., Saba, T., Rahman, S.I.u., Mehmood, Z., Kolivand, H.: Classification of acute lymphoblastic leukemia using deep learning. *Microscopy Research and Technique* **81**(11), 1310–1317 (2018). <https://doi.org/10.1002/jemt.23139>
15. Russakovsky, O., Deng, J., Su, H., Krause, J., Satheesh, S., Ma, S., Huang, Z., Karpathy, A., Khosla, A., Bernstein, M., Berg, A.C., Fei-Fei, L.: ImageNet Large Scale Visual Recognition Challenge. *International Journal of Computer Vision (IJCV)* **115**(3), 211–252 (2015). <https://doi.org/10.1007/s11263-015-0816-y>
16. Shafique, S., Tehsin, S.: Acute lymphoblastic leukemia detection and classification of its subtypes using pretrained deep convolutional neural networks. *Technology in Cancer Research & Treatment* **17**, 1533033818802789 (2018). <https://doi.org/10.1177/1533033818802789>, PMID: 30261827
17. Vogado, L.H.S., Veras, R.D.M.S., Andrade, A.R., Araujo, F.H.D.D., e. Silva, R.R.V., Aires, K.R.T.: Diagnosing leukemia in blood smear images using an ensemble of classifiers and pre-trained convolutional neural networks. In: 2017 30th SIBGRAPI Conference on Graphics, Patterns and Images (SIBGRAPI). pp. 367–373 (Oct 2017). <https://doi.org/10.1109/SIBGRAPI.2017.55>
18. Xie, S., Girshick, R., Dollar, P., Tu, Z., He, K.: Aggregated residual transformations for deep neural networks. In: The IEEE Conference on Computer Vision and Pattern Recognition (CVPR) (July 2017)
19. Yosinski, J., Clune, J., Bengio, Y., Lipson, H.: How transferable are features in deep neural networks? In: Proceedings of the 27th International Conference on Neural Information Processing Systems - Volume 2. pp. 3320–3328. NIPS’14, MIT Press, Cambridge, MA, USA (2014), <http://dl.acm.org/citation.cfm?id=2969033.2969197>